Steady State Operation of Cylindrical Loop Heat Pipe Evaporators

Z. Wang[1], J. M. Ochterbeck[1], J. Perez[2] and P. Rogers[2]
[1] Department of Mechanical Engineering, Clemson University, Clemson, SC, USA
[2] US Army RDECOM-TARDEC, Warren, MI, USA

Abstract

Loop heat pipe evaporators operating under steady state conditions were numerically investigated to describe evaporator characteristics and evaluate evaporator performance. Numerical solutions were obtained for conjugate flow and heat transfer in primary evaporator components. Two geometrical configurations used for cylindrical LHP evaporators, a non-bayonet evaporator and a bayonet evaporator, were considered to examine bayonet effects on evaporator operation. It was found that the presence of a bayonet significantly affects the flow and heat transfer in the liquid core. The influences of input heat flux, inlet liquid sub-cooling, external loop resistance, and effective thermal conductivity of the wick structure on evaporator performance were studied.

1. Introduction

Loop heat pipes (LHPs) are capillary-driven two-phase heat transfer devices capable of transporting large heat loads over long distances. As a robust and passive two-phase thermal transport device, LHP technology is rapidly gaining acceptance in both ground and space applications [1-2]. As shown in Figure 1, the primary LHP components include an evaporator, a compensation chamber, vapor and liquid transport lines, and a condenser. The evaporator is the central part of a LHP which is the heat absorbing component and additionally provides the capillary pumping head for the fluid circulation. The entire loop performance is dependent on the flow and heat transfer characteristics in the evaporator, which mainly include [3]: 1) phase conditions in the wick structure, 2) thermal-fluid behavior in the liquid core, and 3) heat link between the evaporator and the compensation chamber. Physical description of these fundamental flow and heat transfer problems is the key to exploring the loop operational characteristics. The flow and heat transfer in the evaporator are influenced by many factors, such as [4]: 1) applied heat load, 2) level of inlet liquid sub-cooling to the evaporator, 3) wick characteristics, 4) thermo-physical properties of the wick and the working fluid, and 5) evaporator geometry. Hence, development of a model on evaporator operation is needed to physically describe the evaporator characteristics and allow investigation of parameters affecting evaporator performance.

The fluid flow problem is of significant importance in the evaporator and meaningful conclusions are difficult without a combined flow and heat transfer analysis. Most existing models are phenomenological or semi-empirical, which lack sufficient prior knowledge of the fundamental flow and heat transfer characteristics and therefore can not explain the physical mechanisms of many basic phenomena in the evaporator [5]. In order to develop a model for comprehensively describing evaporator behavior and accurately predicting the effects of variations in operational parameters on evaporator operation, fundamentals related to flow and heat transfer in the evaporator must be intensively studied. To date, only a few studies have been reported in this field, and fewer have included these fundamentals in their modeling efforts [1, 4]. In the present study, the steady state operation of cylindrical LHP evaporators was numerically investigated to describe evaporator characteristics and evaluate

Report Documentation Page

Form Approved
OMB No. 0704-0188

1. REPORT DATE	2. REPORT TYPE	3. DATES COVERED
01 AUG 2006	**Journal Article**	**01-08-2006 to 01-08-2006**

4. TITLE AND SUBTITLE	5a. CONTRACT NUMBER
Steady State Operation of Cylindrical Loop Heat Pipe Evaporators	5b. GRANT NUMBER
	5c. PROGRAM ELEMENT NUMBER
6. AUTHOR(S)	5d. PROJECT NUMBER
Paul Rogers; Jeffrey Perez; J. Ochterback; Z. Wang	5e. TASK NUMBER
	5f. WORK UNIT NUMBER
7. PERFORMING ORGANIZATION NAME(S) AND ADDRESS(ES)	8. PERFORMING ORGANIZATION REPORT NUMBER
Clemson University,Department of Mechanical Engineering,Clemson,SC,29631	**; #15838**
9. SPONSORING/MONITORING AGENCY NAME(S) AND ADDRESS(ES)	10. SPONSOR/MONITOR'S ACRONYM(S)
U.S. Army TARDEC, 6501 E.11 Mile Rd, Warren, MI, 48397-5000	**TARDEC**
	11. SPONSOR/MONITOR'S REPORT NUMBER(S)
	#15838

12. DISTRIBUTION/AVAILABILITY STATEMENT

Approved for public release; distribution unlimited

13. SUPPLEMENTARY NOTES

14. ABSTRACT

Loop heat pipe evaporators operating under steady state conditions were numerically investigated to describe evaporator characteristics and evaluate evaporator performance. Numerical solutions were obtained for conjugate flow and heat transfer in primary evaporator components. Two geometrical configurations used for cylindrical LHP evaporators, a non-bayonet evaporator and a bayonet evaporator, were considered to examine bayonet effects on evaporator operation. It was found that the presence of a bayonet significantly affects the flow and heat transfer in the liquid core. The influences of input heat flux, inlet liquid sub-cooling, external loop resistance, and effective thermal conductivity of the wick structure on evaporator performance were studied.

15. SUBJECT TERMS

16. SECURITY CLASSIFICATION OF:			17. LIMITATION OF ABSTRACT	18. NUMBER OF PAGES	19a. NAME OF RESPONSIBLE PERSON
a. REPORT	b. ABSTRACT	c. THIS PAGE			
unclassified	**unclassified**	**unclassified**	**Same as Report (SAR)**	**13**	

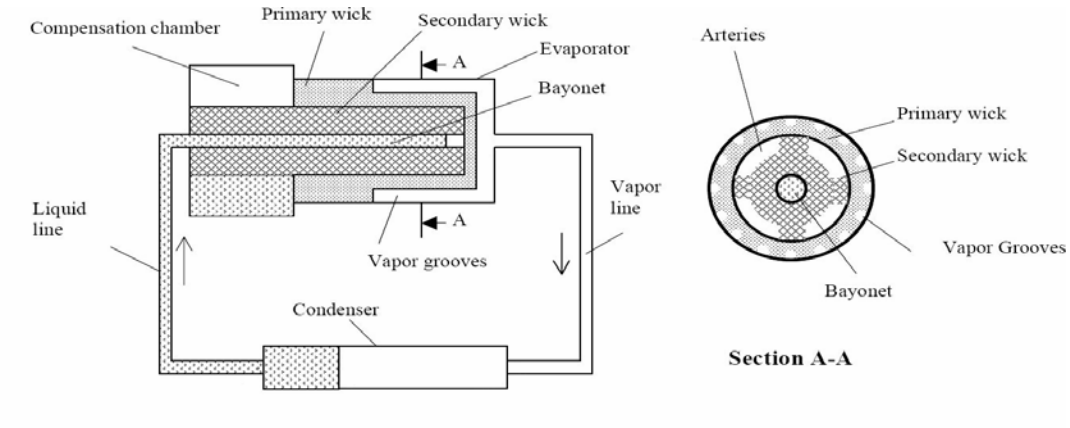

Figure 1- Schematic of the LHP [3]

evaporator behavior. Two typical geometrical configurations used for the cylindrical LHP evaporator, non-bayonet evaporator and bayonet evaporator, were considered to examine the bayonet effects on evaporator operation. Operational parameters affecting flow and heat transfer in the evaporator were also studied to evaluate evaporator performance.

2. Physical Model of the LHP Evaporators

Two types of cylindrical LHP evaporators employed in this study are schematically shown in Figure 2, where the primary difference between these two evaporators is the geometric configuration used for the liquid core in the evaporator. As shown in Figure 2, there are typically two geometric configurations used for the evaporator core in practical applications:

1) Circular core of the non-bayonet evaporator (Figure 2(a)): the extension of the liquid return line serves as the evaporator core.
2) Annular core of the bayonet evaporator (Figure 2(b)): a bayonet is inserted into the liquid core.

In the present study, both configurations were considered to examine the effects of the bayonet on the evaporator operation. The physical model of cylindrical LHP evaporators is shown in Figure 3. For the non-bayonet evaporator, liquid returning from the condenser enters the evaporator through the liquid core. In the circular core, the liquid is drawn into the porous wick due to capillary forces.

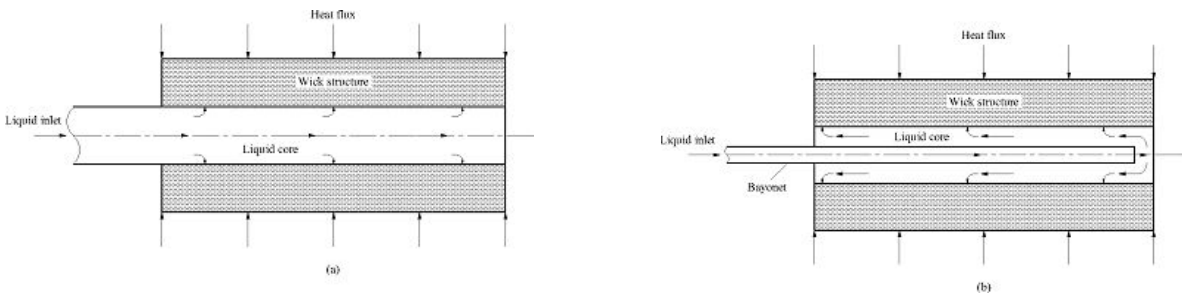

Figure 2- Flow schematic: (a) non-bayonet evaporator and (b) bayonet evaporator.

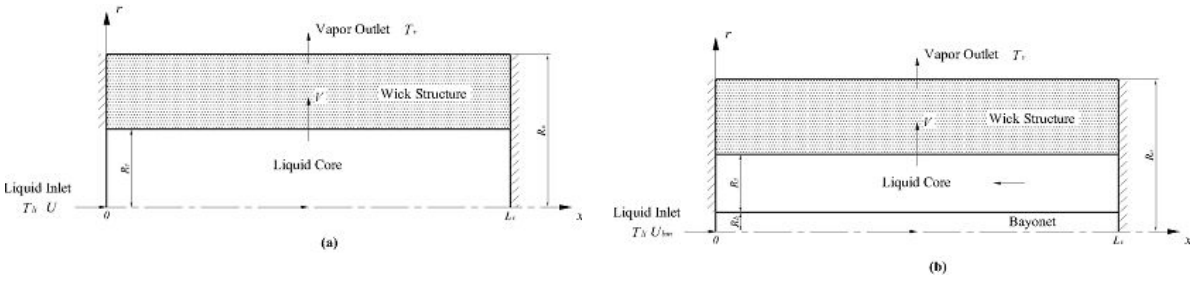

Figure 3- Physical models: (a) non-bayonet evaporator and (b) bayonet evaporator.

The vaporization of liquid takes place at the outer surface of the wick structure. Hence in the non-bayonet evaporator, two distinct computational domains can be defined for the liquid core and the wick structure (see Figure 3(a)). A full-length bayonet was employed in the bayonet evaporator, where the bayonet length is nearly equal to the evaporator length. For such circumstances, three computational domains can be designated: the bayonet, the liquid core and the wick structure in the bayonet evaporator (see Figure 3(b)). At the domain boundaries, the flow and heat transfer are coupled due to the heat and mass connections. In this study, the steady state evaporator operation was numerically simulated as conjugate flow and heat transfer in primary evaporator components. Important assumptions include:

1) For the flow and heat transfer in the evaporator, the thermo-physical properties of the liquid were approximated to be constant and correspond to the saturation temperature in the compensation chamber, T_{cc}.
2) Gravitational effects are neglected.
3) The vapor flow in the vapor channels was neglected.
4) The heat conduction in the cover plate and metal bayonet wall were negligible.

3. Flow and Heat Transfer in the Liquid Core

3.1. Circular Core

The following major assumptions were made for the flow and heat transfer in the circular core, as shown in Figure 3(a):

1) The liquid flow in the liquid core is incompressible and laminar.
2) Since the flow in the liquid return line is fully developed and adiabatic, it was assumed that the flow at the inlet of the liquid core is fully developed and the inlet temperature is uniform.
3) The outlet velocity at the wick/core interface is uniform.

Governing Equations

Continuity: $$\frac{\partial u}{\partial x}+\frac{1}{r}\frac{\partial}{\partial r}(rv)=0 \quad (1)$$

Momentum: $$\frac{\partial(u^2)}{\partial x}+\frac{1}{r}\frac{\partial(ruv)}{\partial r}=-\frac{1}{\rho_l}\frac{\partial P}{\partial x}+\nu_l\left[\frac{\partial^2 u}{\partial x^2}+\frac{1}{r}\frac{\partial}{\partial r}\left(r\frac{\partial u}{\partial r}\right)\right] \quad (2)$$

$$\frac{\partial(uv)}{\partial x}+\frac{1}{r}\frac{\partial(rv^2)}{\partial r}=-\frac{1}{\rho_l}\frac{\partial P}{\partial r}+\nu_l\left[\frac{\partial^2 v}{\partial x^2}-\frac{v}{r^2}+\frac{1}{r}\frac{\partial}{\partial r}\left(r\frac{\partial v}{\partial r}\right)\right] \quad (3)$$

Energy: $$\frac{\partial(uT)}{\partial x}+\frac{1}{r}\frac{\partial(rvT)}{\partial r}=\alpha_l\left[\frac{\partial^2 T}{\partial x^2}+\frac{1}{r}\frac{\partial}{\partial r}\left(r\frac{\partial T}{\partial r}\right)\right] \quad (4)$$

Boundary Conditions

At $x=0$: $u(r)=2U\left[1-\left(\frac{r}{R_i}\right)^2\right]$ (5); $v=0$ (6); $T=T_{li}$ (7)

At $x=L_e$: $u=0$ (8); $v=0$ (9); $\frac{\partial T}{\partial x}=0$ (10)

At $r=0$: $\frac{\partial u}{\partial r}=0$ (11); $v=0$ (12); $\frac{\partial T}{\partial r}=0$ (13)

At $r=R_i$: $u=0$ (14); $v=\frac{R_i}{2L_e}U$ (15)

In Equation (5), the mean velocity, U, in the liquid core can be obtained by performing an overall heat balance on the evaporator as: $U=\frac{1}{\rho_l R_i^2}\frac{2R_o L_e q''_w}{h_{fg}+c_p(T_v-T_{li})}$ (16)

Two saturation states exist for LHP operation: one situates at the evaporating interface in the evaporator grooves while another saturation state which represents the compensation chamber exists in the liquid return line [3]. Because these two saturation states are thermodynamically related, the following condition must be satisfied for the loop system [6]: $\Delta P_{tot}-\Delta P_w=\left(\frac{\partial P}{\partial T}\right)_{sat}(T_v-T_{cc})$ (17), where the slope of the vapor-pressure curve, $(\partial P/\partial T)_{sat}$, can be related to thermo-physical properties by using the Clapeyron equation (18), thus, T_v can be written as (19):

$$\left(\frac{\partial P}{\partial T}\right)_{sat}=\frac{h_{fg}}{T_{sat}\Delta v_{fg}}. \quad (18) \qquad T_v=T_{cc}\left(1+\frac{\Delta v_{fg}}{h_{fg}}\Delta P_{ext}\right), \quad (19)$$

where the external loop resistance $\Delta P_{ext}=\Delta P_{tot}-\Delta P_w$.

3.2. Annular Core

In practical applications, a bayonet core design is often utilized for the LHP evaporator, where a bayonet is inserted into the liquid core. As shown in Figure 2(b), liquid returning from the condenser flows inside the bayonet and then flows back into the annular core between the bayonet and the wick. Compared with the circular core, this reverses the main flow direction in the liquid core and thus moves the stagnation point from the vapor end to the liquid end where the liquid in the bayonet has maximum sub-cooling. As a consequence, this configuration forces any vapor present in the liquid core to flow to the inlet section of the

evaporator where it can be collapsed by exchanging heat with the incoming sub-cooled liquid or vented to the compensation chamber. During liquid flow in the liquid core, liquid is drawn into the porous wick due to capillary forces. As shown in Figure 3(b), the same governing equations (1) to (4) can be still applied for the flow and heat transfer in the annular core with new boundary conditions:

At $x = 0$: $u = 0$ (20); $v = 0$ (21); $\frac{\partial T}{\partial x} = 0$ (22)

At $x = L_e$: $u = U_{ci}$ (23); $v = 0$ (24)

At $r = R_b$: $u = 0$ (25); $v = 0$ (26)

At $r = R_i$: $u = 0$ (27); $v = V = -\frac{R_i^2 - R_b^2}{2R_i L_e} U_{ci}$ (28)

Due to the presence of the bayonet, the stagnation end of the annular core situates at the liquid inlet end of the evaporator. In Equation (23), the inlet velocity, U_{ci}, in the liquid core is given by: $U_{ci} = -\frac{2R_o L_e q_w'' / \rho_l \left(R_i^2 - R_b^2\right)}{h_{fg} + c_p \left(T_v - T_{li}\right)}$ (29).

4. Heat and Mass Connections between Components

For fully developed laminar flow in the bayonet, the following parabolic velocity profile can be obtained: $u(r) = 2U_{bm}\left[1 - \left(\frac{r}{R_i}\right)^2\right]$ (30), where the mean velocity, U_{bm}, in the bayonet and the energy equation for the flow and heat transfer in the bayonet can be expressed as: $U_{bm} = \frac{1}{\rho_l R_b^2} \frac{2R_o L_e q_w''}{h_{fg} + c_p \left(T_v - T_{li}\right)}$ (31), $u\frac{\partial T}{\partial x} = \alpha_l \left[\frac{\partial^2 T}{\partial x^2} + \frac{1}{r}\frac{\partial}{\partial r}\left(r\frac{\partial T}{\partial r}\right)\right]$ (32)

The boundary conditions for the bayonet are given by:

At $x = 0$: $T = T_{li}$ (33) and At $r = 0$: $\frac{\partial T}{\partial r} = 0$ (34)

For the wick structure, the following major assumptions were made:

1) The porous wick is rigid, homogeneous, and isotropic.
2) The wick is fully saturated with liquid, where vaporization of the liquid takes place exclusively from the outer surface of the wick.
3) Darcy's law is applicable to the liquid flow in the wick structure.
4) The liquid and solid phases are in local thermal equilibrium.
5) The temperature at the outer surface of the wick is nearly equal to the vapor temperature in the vapor grooves.

Governing Equations

Continuity: $\frac{\partial u}{\partial x} + \frac{1}{r}\frac{\partial}{\partial r}(rv) = 0$ (35)

Momentum: $u = -\frac{K}{\mu}\frac{\partial P}{\partial x}$ (36); $v = -\frac{K}{\mu}\frac{\partial P}{\partial r}$ (37)

Energy: $u\frac{\partial T}{\partial x} + v\frac{\partial T}{\partial r} = \alpha_{eff}\left[\frac{\partial^2 T}{\partial x^2} + \frac{1}{r}\frac{\partial}{\partial r}\left(r\frac{\partial T}{\partial r}\right)\right]$ (38)

Boundary Conditions

At $x = 0$: $u = 0$ (39); $\frac{\partial T}{\partial x} = 0$ (40) At $x = L_e$: $u = 0$ (41); $\frac{\partial T}{\partial x} = 0$ (42)

At $r = R_i$: $u = 0$ (43); $v = V$ (44) At $r = R_o$: $u = 0$ (45); $T = T_v$ (46)

The above boundary conditions suggest that the axial velocity component in the wick structure is zero. Thus, the velocity profile in the wick structure can be directly determined by the continuity equation as $u = 0$ (47) and $v = \frac{R_i}{r}V$ (48). Therefore, the energy equation (38) becomes $v\frac{\partial T}{\partial r} = \alpha_{eff}\left[\frac{\partial^2 T}{\partial x^2} + \frac{1}{r}\frac{\partial}{\partial r}\left(r\frac{\partial T}{\partial r}\right)\right]$ (49).

Therefore, the steady state evaporator operation was solved as a conjugate problem of flow and heat transfer in the bayonet, the liquid core and the wick structure, where the flow and heat transfer in each domain can be coupled by conjugate boundary conditions at domain boundaries. Conjugate boundary conditions exist at the core/bayonet interface ($r = R_b$) and the wick/core interface ($r = R_i$), where temperatures and heat fluxes at the boundaries on both sides should be equal. Assuming that the heat transfer in the bayonet wall is negligible these boundary conditions can be expressed as:

At $r = R_b$: $T\big|_{r=R_b^-} = T\big|_{r=R_b^+}$ (50); $\left.\frac{\partial T}{\partial r}\right|_{r=R_b^-} = \left.\frac{\partial T}{\partial r}\right|_{r=R_b^+}$ (51)

At $r = R_i$: $T\big|_{r=R_i^-} = T\big|_{r=R_i^+}$ (52); $\lambda_l\left.\frac{\partial T}{\partial r}\right|_{r=R_i^-} = \lambda_{eff}\left.\frac{\partial T}{\partial r}\right|_{r=R_i^+}$ (53)

7. Numerical Treatment

A finite difference method was used to solve the governing equations for the flow and heat transfer in the bayonet, the liquid core, and the wick structure. A uniform staggered grid mesh was used in the present study. The finite difference equations were formulated using the control volume approach, where the power law scheme [7] was applied to represent the transport properties on the control volume surfaces. Due to unknown boundary conditions at both the wick/core and core/bayonet interfaces, the temperature fields were solved as a conjugate problem. The convergence criterion of the numerical solution for the velocity and temperature fields was that the relative errors between two consecutive iterations are less than 10^{-8}. The total mass and energy balances were also ensured to be within 0.1% error after convergence was achieved.

8. Results and Discussions

Numerical calculations were carried out for cylindrical LHP evaporators (including non-bayonet and bayonet designs) with the following parameters:

a) Working fluid: ammonia ($T_{cc} = 300K$)
b) Wick inner and outer radii: $R_i = 6mm$, $R_o = 12mm$
c) Bayonet outer radius for the bayonet evaporator: $R_b = 1.5mm$
d) Evaporator length: $L_e = 50mm$
e) Input heat flux: $q''_w = 20kW/m^2$, $30\,kW/m^2$ and $50\,kW/m^2$
f) Inlet liquid sub-cooling: $\Delta T_{sub.li} = T_{cc} - T_{li} = 5K$ and $10K$
g) Wick effective thermal conductivity: $\lambda_{eff} = 10W/m \cdot K$ and $1W/m \cdot K$
h) External loop resistance: $\Delta P_{ext} = 40kPa$ (or T_v = 301.25 K) and $\Delta P_{ext} = 10kPa$ (or $T_v = 300.3125K$)

A representative solution of the temperature distribution in the non-bayonet evaporator is shown in Figure 4. At the inlet of the liquid core, the temperature is uniform and equal to 295K. In the liquid core, the temperature increases gradually along the main flow direction and also increases monotonically with the radial position. As a result, the maximum temperature appears at the far end of the wick/core interface ($r = 6mm$). A representative solution of the flow and heat transfer in the bayonet evaporator is shown in Figures 5 to 7. Figure 5 illustrates the temperature distribution in the bayonet which is significantly influenced by the heat exchange between the bayonet and the liquid core. In the center region of the bayonet, the temperature gradually increases along the main flow direction due to the heat transfer from the liquid core to the bayonet while the temperature profile close to the bayonet wall is directly affected by the temperature field in the liquid core. It can be concluded that the sub-cooled liquid in the bayonet serves to be a heat sink for the liquid core, especially the liquid at the inlet of the bayonet which has the maximum sub-cooling level.

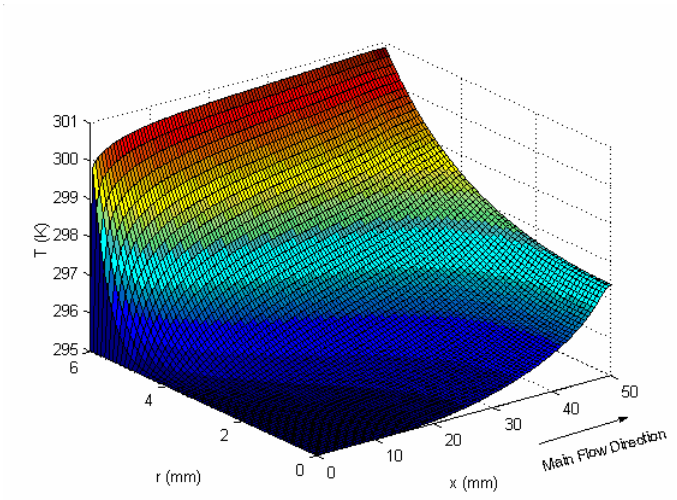

Figure 4 - Temperature distribution in the circular core ($q''_w = 30kW/m^2$, $\Delta T_{sub.li} = 5K$, $\lambda_{eff} = 10W/m \cdot K$, $\Delta P_{ext} = 40kPa$)

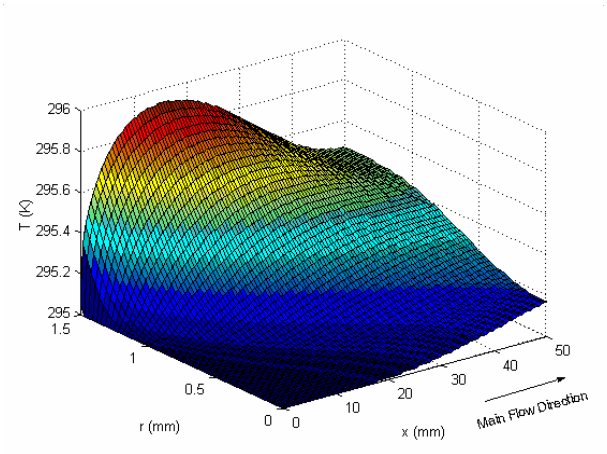

Figure 5- Temperature distribution in the bayonet ($q''_w = 30kW/m^2$, $\Delta T_{sub.li} = 5K$, $\lambda_{eff} = 10W/m \cdot K$, $\Delta P_{ext} = 40kPa$)

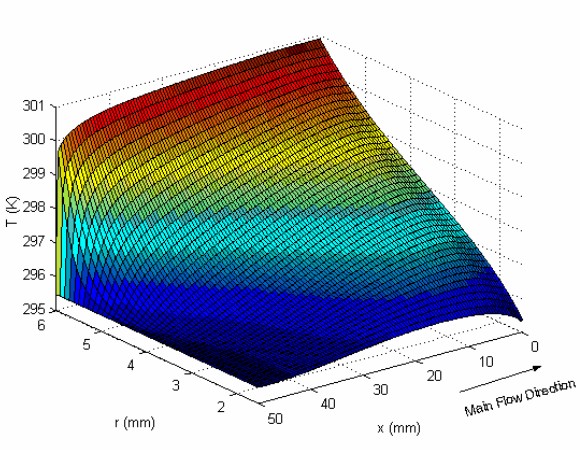

Figure 6- Temperature distribution in the liquid core ($q''_w = 30kW/m^2$, $\Delta T_{sub.li} = 5K$, $\lambda_{eff} = 10W/m \cdot K$, $\Delta P_{ext} = 40kPa$)

Figure 6 shows the temperature distribution in the liquid core. Liquid exiting from the bayonet immediately enters the annular core with a nearly uniform temperature. In the liquid core, the liquid is heated by the wick surface, where the temperature near the wick surface increases gradually along the flow direction and also increases monotonically with the radial position.

It can be also observed from Figure 6 that the temperature near the bayonet increases initially and drops afterwards along the flow direction. This behavior is due to the fact that there is heat dissipation from the liquid core to the bayonet. Figure 7 shows the temperature distribution in the wick structure. In the wick structure, the temperature gradually increases along the liquid flow direction.

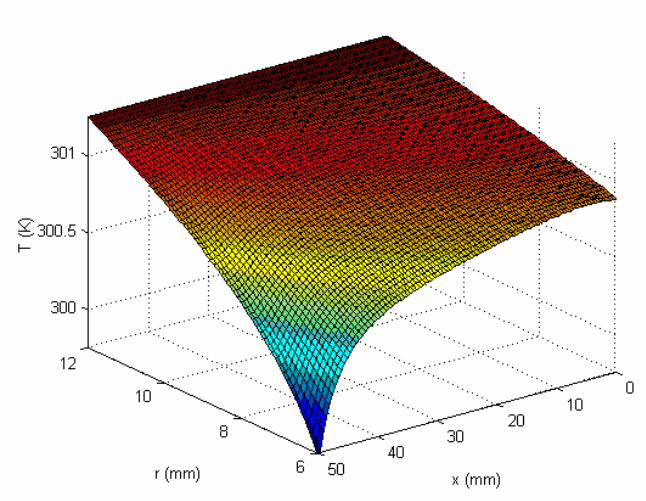

Figure 7- Temperature distribution in the wick structure ($q''_w = 30kW/m^2$, $\Delta T_{sub.li} = 5K$, $\lambda_{eff} = 10W/m \cdot K$, $\Delta P_{ext} = 40kPa$)

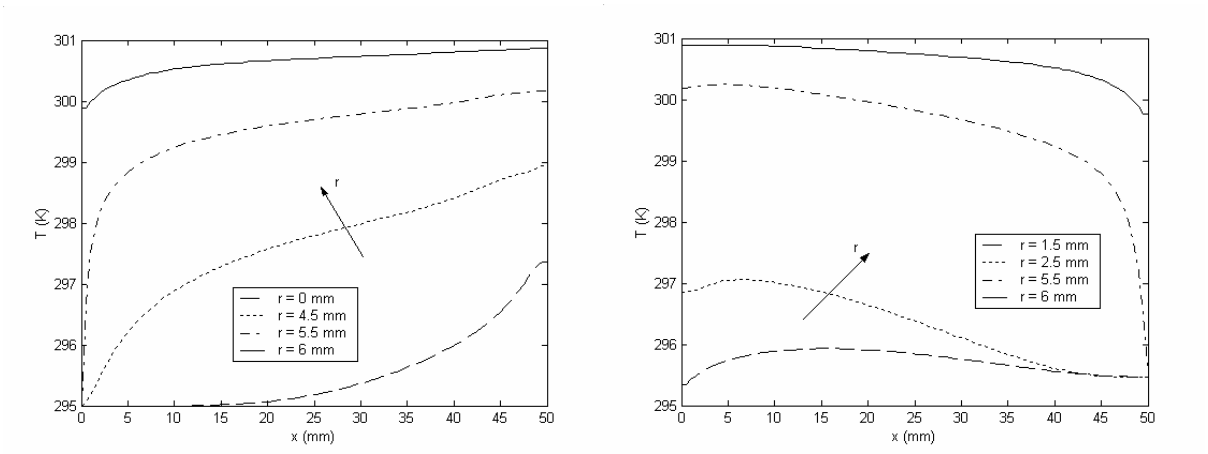

(a) (b)

Figure 8- Variations of temperature profile in the radial position ($q''_w = 30kW/m^2$, $\Delta T_{sub.li} = 5K$, $\lambda_{eff} = 10W/m \cdot K$, $\Delta P_{ext} = 40kPa$): (a) circular core and (b) annular core

8.1. Bayonet effects

Figure 8 shows that the temperature distribution in the annular core is similar to that in the circular core except the temperature reverses in the x-direction. Consequently, the maximum temperature appears at the liquid end ($x = 0$) in the annular core while it appears at the vapor end ($x = L_e$) in the circular core (see Figure 9). Comparisons of the results of flow and heat transfer in the circular core and annular core lead to the following conclusions for bayonet effects on evaporator operation:

1) "Reversal" Effect (x-direction): the presence of a bayonet reverses the main flow direction in the liquid core, and thus reverses the temperature field (see Figure 9).
2) "Cooling" Effect (r-direction): for the circular core, the liquid is heated along the flow direction and the temperature gradually increases (see Figure 8(a)). However in the annular core, the liquid is cooled by the sub-cooled liquid in the bayonet as well as heated by the wick surface. It can be also observed from Figure 8(b) that this "cooling" effect is obvious only in the region close to the bayonet. For the region far from the bayonet, this effect tends to attenuate, and finally it vanishes in the wick structure.

Due to the above effects, the presence of a bayonet forces any vapor present in the liquid core to flow to the inlet liquid end of the evaporator where it can be collapsed by exchanging heat with the incoming sub-cooled liquid in the bayonet.

8.2. Heat Flux Effects

The temperature profiles at the domain boundaries, including the wick/core interface and core/bayonet interface, give a good representation for the flow and heat transfer characteristics in the evaporator, which includes sufficient flow and heat transfer information, such as heat exchange between each flow domain, the thermal-fluid behavior in the liquid core and the cooling capability of the liquid in the bayonet.

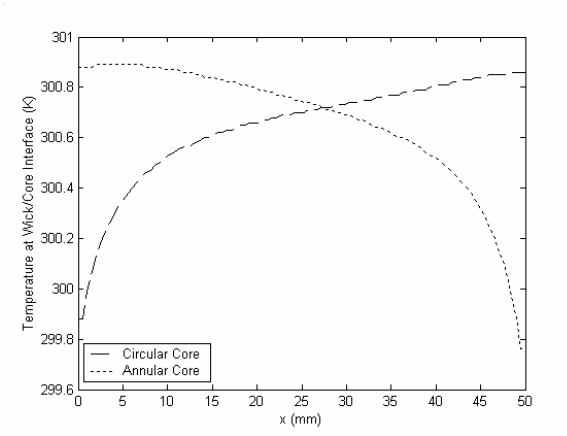

Figure 9- Comparison of temperature distributions at the wick/core interface ($q''_w = 30kW/m^2$, $\Delta T_{sub.li} = 5K$, $\lambda_{eff} = 10W/m \cdot K$, $\Delta P_{ext} = 40kPa$)

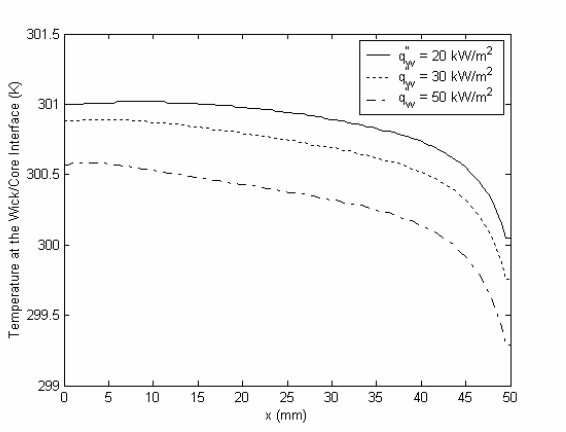

Figure 10 - Influence of heat flux on temperature at the wick/core interface ($\Delta T_{sub.li} = 5K$, $\lambda_{eff} = 10W/m \cdot K$, $\Delta P_{ext} = 40kPa$)

Figure 10 shows the effect of heat flux on the temperature at the wick/core interface, where the temperature decreases with the input heat flux. The temperature at the wick/core interface is highly related to the heat leak from the wick to the liquid core. Increasing the heat flux increases the system mass flow rate and thus increases the convective effects. As a result, the heat conduction to the liquid core decreases. It is also seen from Figure 10 that the temperature at the stagnation point ($x = 0$) is greater than the saturation temperature ($T_{cc} = 300K$), which indicates possible vapor formation on the inner surface of the wick. Increasing the heat flux decreases the maximum temperature in the liquid core and helps to prevent vapor formation. Figure 11 shows the effect of heat flux on the temperature at the core/bayonet interface, where the temperature also decreases with the heat flux. The temperature at the core/bayonet interface is highly involved with the heat dissipation from the liquid core to the bayonet and gives a good representation for the cooling capability of the sub-cooled liquid in the bayonet. Increasing the heat flux increases the mass flow rate in the bayonet and thus increases the cooling capability.

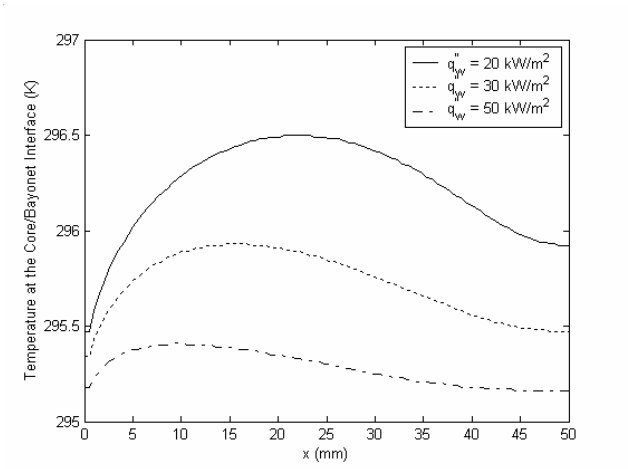

Figure 11 - Influence of heat flux on temperature at the core/bayonet interface ($\Delta T_{sub.li} = 5K$, $\lambda_{eff} = 10W/m \cdot K$, $\Delta P_{ext} = 40kPa$)

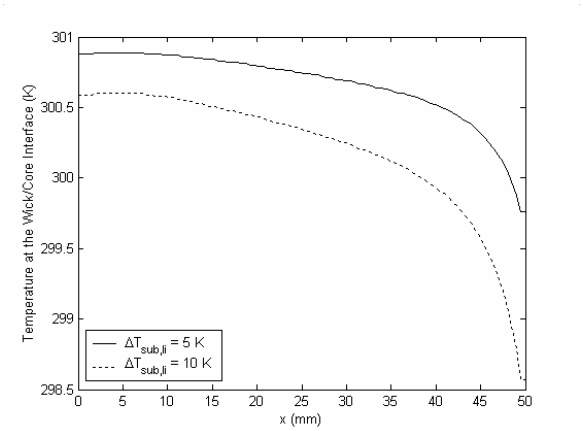

Figure 12- Influence of inlet liquid sub-cooling on temperature at the wick/core interface ($q''_w = 30kW/m^2$, $\lambda_{eff} = 10W/m \cdot K$, $\Delta P_{ext} = 40kPa$)

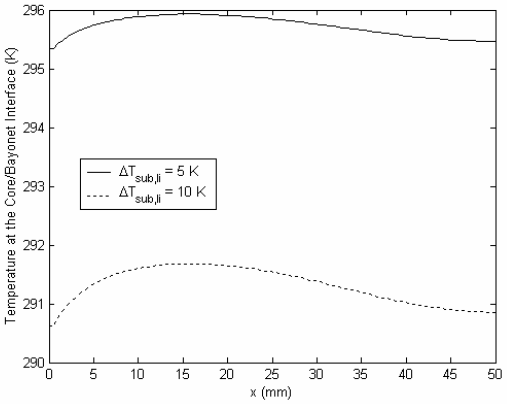

Figure 13- Influence of inlet liquid sub-cooling on temperature at the core/ bayonet interface($q''_w = 30kW/m^2$, $\lambda_{eff} = 10W/m \cdot K$, $\Delta P_{ext} = 40kPa$)

8.3. Liquid Sub-cooling Effects

Figures 12 and 13 present the influence of inlet liquid sub-cooling on the evaporator operation. Figure 12 shows the liquid sub-cooling effects on the temperature at the wick/core interface. Figure 13 shows the effect of inlet liquid sub-cooling on the temperature at the core/bayonet interface. As seen, the liquid sub-cooling has a significant influence on the cooling effect of the sub-cooled liquid in the bayonet. Increasing liquid sub-cooling greatly decreases the temperature at the core/bayonet interface, which means that the cooling capability of the liquid in the bayonet is significantly enhanced by the increase of the inlet liquid sub-cooling.

8.4. External Loop Resistance Effects

Figures 14 and 15 show the influence of external loop resistance on the flow and heat transfer in the evaporator. The effect of external resistance on the temperature at the wick/core interface is shown in Figure 14, where the temperature at the wick/core interface increases with the external loop resistance. For a given saturation temperature in the compensation chamber, Equation (19) indicates that the vapor saturation temperature in the vapor channels is determined by the external loop resistance. Increasing the external loop resistance increases the temperature at the outer surface of the wick and thus increases the heat load imposed on the wick surface. As a consequence, the heat transfer from the wick to the liquid core increases. Figure 14 also indicates that the liquid in the liquid core is sub-cooled for an external resistance of 10 kPa. When the external resistance is increased to 40 kPa, it is observed that the liquid at the outlet of the liquid core becomes superheated, which means that vapor may be generated in the liquid core under such a condition. Figure 15 shows that the temperature at the core/bayonet interface slightly increases with external resistance.

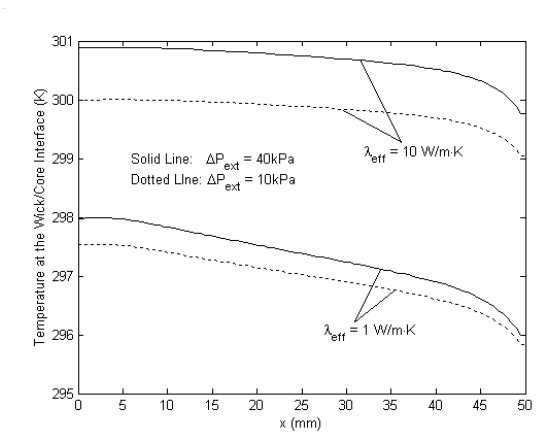

Figure 14- Influence of λ_{eff} and ΔP_{ext} on temperature at the wick/core interface ($q''_w = 30kW/m^2$, $\Delta T_{sub.li} = 5K$)

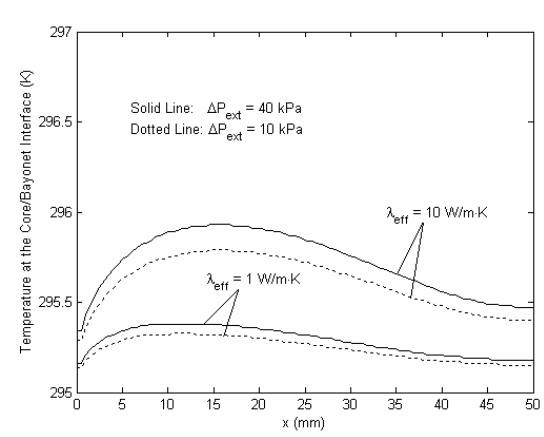

Figure 15- Influence of λ_{eff} and ΔP_{ext} on temperature at the core/bayonet interface ($q''_w = 30kW/m^2$, $\Delta T_{sub.li} = 5K$)

8.5. Effective Thermal Conductivity Effects

Figures 14 and 15 also illustrate the influence of the effective thermal conductivity on the temperature at the wick/core interface and the temperature at the core/bayonet interface, respectively. Figure 14 shows the effect of effective thermal conductivity on the temperature at the wick/core interface. Increasing effective thermal conductivity increases the heat transfer to the core, and thus increases the temperature at the wick/core interface. Figure 14 also suggests that the liquid core is more vulnerable to vapor formation for the wick structure with a higher effective thermal conductivity. As shown in Figure 14, the temperature at the wick/core interface is much lower than the saturation temperature for an effective thermal conductivity of $1\,W/m\cdot K$ while it is greater than the saturation temperature for an effective thermal conductivity of $10\,W/m\cdot K$. Figure 15 shows the effect of effective thermal conductivity on the temperature at the core/bayonet interface. Increasing effective thermal conductivity increases the heat transfer to the core, and accordingly increases the heat dissipation from the core to the bayonet. As a result, the temperature in the bayonet increases with the effective thermal conductivity, as shown in Figure 15.

9. Conclusions

Loop heat pipe evaporators operating under steady state conditions were numerically investigated to describe evaporator characteristics and evaluate evaporator performance. The numerical results indicated that in the liquid core the maximum temperature appears at the stagnation point of the wick/core interface, where the vapor may be generated on the inner wick surface. The sub-cooled liquid in the bayonet serves to be a heat sink for the liquid core, especially the liquid at the inlet of the bayonet which has the maximum sub-cooling level. Two typical geometrical configurations used for the cylindrical LHP evaporator, non-bayonet evaporator and bayonet evaporator, were considered to examine the bayonet effects on evaporator operation. It was found that the presence of a bayonet forces any vapor present in the liquid core to flow to the inlet liquid end of the evaporator where it can be collapsed by exchanging heat with the incoming sub-cooled liquid in the bayonet.

The presence of a bayonet significantly affects the flow and heat transfer in the liquid core and helps to prevent vapor bubbles from accumulating inside the core, which must be considered in the model.

References

[1] Yu.F. Maidanik, State-of-the-art of CPL and LHP technology, in: Heat Pipe Science and Technology, Proceedings of 11th International Heat Pipe Conference, Tokyo, 1999, pp. 19-30.

[2] J.M. Ochterbeck, Heat pipes, in: A. Bejan and A. Kraus (Eds.), Handbook of Heat Transfer, John Wiley & Sons, New York, 2003, pp. 1181-1230.

[3] J. Ku, Operating characteristics of loop heat pipes, SAE Paper No. 1999-01-2007, July 1999.

[4] Y.H. Yan, J.M. Ochterbeck, Numerical investigation of the steady-state operation of a cylindrical capillary pumped loop evaporator, Journal of Electrical Packaging 125(3) (2003), 251-260.

[5] A. Faghri, Heat Pipe Science and Technology, Taylor & Francis, Washington DC, 1995.

[6] Y.F. Maidanik, Y.G. Fershtater, Theoretical basis and classification of loop heat pipes and capillary pumped loops, Proc. 10th International Heat Pipe Conf., Stuttgart, Germany, 1997.

[7] S.V. Patankar, Numerical Heat Transfer and Fluid Flow, McGraw-Hill, New York.

Nomenclature					
h_{fg}	Latent Heat [kJ/kg]	K	Permeability [m^2]	L	Length [m]
P	Pressure [Pa]	q''	Heat Flux [kW/m^2]	x,r	Cooridnates in Domain
T	Temperature [K]	u	Axial Velocity [m/s]	v	Radial Velocity [m/s]
v	Specific Volume [m^3/kg]	U	Inlet Velocity [m/s]	α	Thermal Diffusivity [m^2/s]
μ	Viscosity [N s/m^2]	ρ	Density [kg/m^3]	b	Bayonet
c	Capillary, Liquid Core	cc	Compensation Chamber	e	Evaporation
eff	Effective	evp	Evaporator	ext	External
i	Interface, Inlet, Inner	l	Liquid	m	Meniscus
o	Outer	p	Pore, Particle	sat	Saturation
tot	Total	v	Vapor	w	Solid Wall, Wick